IEEE Access
Multidisciplinary | Rapid Review | Open Access Journal

Received April 22, 2018, accepted May 26, 2018, date of publication May 31, 2018, date of current version June 29, 2018.

Digital Object Identifier 10.1109/ACCESS.2018.2842198

Generalized Extended State Observer Based High Precision Attitude Control of Quadrotor Vehicles Subject to Wind Disturbance

DI SHI[1], ZHONG WU[1], AND WUSHENG CHOU[2,3]

[1]School of Instrumentation Science and Optoelectronics Engineering, Beihang University, Beijing 100191, China
[2]School of Mechanical Engineering and Automation, Beihang University, Beijing 100191, China
[3]State Key Laboratory of Virtual Reality Technology and Systems, Beihang University, Beijing 100191, China

Corresponding author: Zhong Wu (wuzhong@buaa.edu.cn)

This work was supported by the State Key Development Program for Basic Research of China under Grant 2013CB035503.

ABSTRACT Wind disturbance may significantly degrade the attitude control performance during the flight of quadrotor vehicles. In order to meet the requirement of high-precision attitude control, a generalized extend state observer (GESO)-based disturbance and uncertainty estimation and attenuation control strategy is proposed in this paper. First, the disturbances are considered as a time polynomial function, and the *n*th order model of disturbances are augmented into the quadrotor dynamics. According to the reconstructed model, a GESO is designed and its stability is proved by the Lyapunov theory. Then, we analyze the influences of the observer order and bandwidth on the estimation accuracy in detail and give the gain tuning guidelines for GESO. Second, we design an attitude tracking controller based on the backstepping method and discuss the stability of the entire system. Finally, the numerical simulations and real-time experiments are carried out to evaluate the performance of the proposed controller with the GESO of different orders. Our results show that the proposed method can achieve precise attitude tracking for a quadrotor subject to wind disturbance. Furthermore, when the bandwidth of the GESO is fixed, the performance of the proposed controller improves with the increases of the GESO order.

INDEX TERMS Quadrotor, high precision, GESO, wind disturbance, attitude control.

I. INTRODUCTION

In recent years, the research on the quadrotor vehicles attracts great interest due to the wide range of civil and military applications, and a lot of achievements have been made [1]–[3]. As a new kind of unmanned aerial vehicle (UAV), quadrotor is a small rotorcraft with four propellers driven by four direct current (DC) motors respectively [4]. Compared with traditional helicopters, the structure of quadrotor is simpler and more efficient, and has significant advantages in precise hovering, aggressive maneuver, vertical take-off and landing (VTOL) [5], [6], *etc.*

In order to meet the mission requirements of the quadrotor, high precision attitude control is essential. However, when operating in outdoor environments, quadrotors would be easily affected by wind field [7], which is a component of external disturbances, during the course of flight. Moreover, the quadrotor is an underactuated and nonlinear coupled system [8]. Therefore, it is difficult for the traditional linear controllers [9]–[11] to achieve the high precision control under the influence of disturbances. To solve these problems, many approaches have been proposed in literatures. Robust adaptive controller can effectively eliminate the influence of system model uncertainties [12], except that it is too conservative in control performance. Sliding mode method is used to control the inner loop of the aircraft, and ensured good attitude tracking performance [13], [14]. However, chattering is inevitable in this method.

Alternatively, the disturbances can be accurately estimated and attenuated in the feedforward loop [15]. The disturbance and uncertainty estimation and attenuation (DUEA) strategy would be a potential solution. Those methods have been widely explored and used in recent years [16], [17]. The DUEA framework can be divided into two parts, namely, a disturbance and uncertainty estimator (DUE) and a feedback controller (FC). In the first part, DUE is designed to estimate the disturbances so that they could be compensated in the feedforward loop. Then the FC in the second part is designed to guarantee fast

2169-3536 © 2018 IEEE. Translations and content mining are permitted for academic research only.
Personal use is also permitted, but republication/redistribution requires IEEE permission.
See http://www.ieee.org/publications_standards/publications/rights/index.html for more information.

convergence of the closed-loop system. Under the framework of DUEA strategy, the DUE plays a very important role, because the performance of the closed-loop system is largely determined by the estimate from the DUE. A series of observers have been proposed as the DUE so far, such as disturbance observer (DO) [18], [19], extended state observer (ESO) [20]–[22] and proportional integral observer (PIO) [23], [24] *etc.* By the appropriate use of the observer, disturbance rejection performance and robustness of the existing control system could be significantly improved.

Consequently, a lot of improvements on the DUE are made in literatures. Sliding mode technology is a good choice due to its attractive properties such as its insensitivity with respect to unknown inputs and finite time convergence to the exact values of the state vectors. In [25], a sliding model disturbance observer (SMDO) was used to estimate the quadrotor velocities, the external disturbances such as wind and parameter uncertainties, and achieves good results, while chattering was serious. To solve this problem, higher order sliding mode differentiation was used in [26], resulting in less chattering. Except for sliding mode technologies, high order method is also used in design of the DUE. In [27], the extended disturbance observer (EDO) was proposed to handle a larger class of mismatched uncertainties. Higher order EDO was applied for attitude stabilization of flexible spacecrafts, and the efforts of different orders on the performance of EDO were investigated [28]. In [29], a generalized proportional integral observer (GPIO) was designed to estimate the time varying disturbances which were approximated by a Taylor polynomial, and showed a better disturbance rejection property compared with DOB and PIO. In [30], the generalized ESO with high order was investigated. It is shown that if the chosen observer bandwidth is much larger than the frequency of the disturbance, the proposed ESO would offer better state estimation accuracy in comparison with the conventional first order ESO, when dealing with the fast varying sinusoidal disturbances. Moreover, in [31], an enhanced generalized ESO was designed by introducing the equivalent disturbance model so that the perturbation terms of the observer can be decreased, and achieved a good estimation accuracy. However, it is difficult to get the accurate model of disturbance in some applications, which will have certain effect on the robustness of the system.

In this paper, ESO method is adopted because of its less dependence on model information [32], [33]. As the disturbances acting on the quadrotor are time varying, stochastic and nonlinear, we generally approximate them as a form of time polynomials and then develop a GESO, instead of the traditional one, to address this problem. The main contribution of this work is threefold:

(1) Design and implementation of a GESO for the high precision attitude control of quadrotor vehicles based on the augmented dynamic model, and the stability analysis of the entire system including DUE and FC.
(2) Analysis of the influences of the observer order and bandwidth on the estimation accuracy, and the gain tuning guidelines for GESO.
(3) From a practical perspective, proposal for the observer order and bandwidth combination of the GESO that works well on real systems according to our experiments.

The outline of this work is as follows: Some preliminaries are presented in Section II. The mathematical model and the control problems of quadrotor are formulated in Section III. A GESO is designed in Section IV, as well as the proof of stability and the gain tuning guidelines are also given in this section. In section V, an attitude tracking controller is designed via the backstepping method. Numerical simulation and real time experimental results are presented in Section VI, and the conclusions are summarized in Section VII.

II. PRELIMINARIES

A. NOTATIONS

Throughout this paper, the following notations will be used. $\mathbb{R}$ is the set of real numbers. Let $\|\cdot\|$ denote the 2-norm of a vector or a matrix. For a given vector $\boldsymbol{v} = [v_1, \ldots, v_n]^T \in \mathbb{R}^n$, $||\boldsymbol{v}|| = \sqrt{\boldsymbol{v}^T\boldsymbol{v}}$, and for a given matrix $\boldsymbol{A} \in \mathbb{R}^{n\times n}$, $||\boldsymbol{A}|| = \sqrt{\lambda_{\max}\left(\boldsymbol{A}^T\boldsymbol{A}\right)}$, where $\lambda_{\max}(\cdot)$ is the maximal eigenvalue of the matrix. In addition, the operator $S(\cdot)$ maps a vector $\boldsymbol{x} = [\,x_1\ x_2\ x_3\,]^T$ to a skew symmetric matrix as:

$$S(\boldsymbol{x}) = \begin{bmatrix} 0 & -x_3 & x_2 \\ x_3 & 0 & -x_1 \\ -x_2 & x_1 & 0 \end{bmatrix} \tag{1}$$

When one says that vector function $\boldsymbol{f}(\boldsymbol{x}) \in \mathbb{R}^n$ is Lipschitz continuous, it means that each element of $\boldsymbol{f}(\boldsymbol{x})$, *i.e.*, $f_i(x)$ is Lipschitz continuous.

B. QUATERNION OPERATIONS

In order to avoid the singularity problem of trigonometric functions, unit quaternion $\boldsymbol{q} = \left[\,q_0\ \boldsymbol{q}_v^T\,\right]^T \in \mathbb{R}^4$, $\|\boldsymbol{q}\| = 1$ is used to represent rotation [34]. Following are the operations we used.

The quaternion multiplication is:

$$\boldsymbol{q}_1 \otimes \boldsymbol{q}_2 = \begin{bmatrix} q_{01}q_{02} - \boldsymbol{q}_{v1}^T\boldsymbol{q}_{v2} \\ q_{01}\boldsymbol{q}_{v2} + q_{02}\boldsymbol{q}_{v1} - S(\boldsymbol{q}_{v2})\boldsymbol{q}_{v1} \end{bmatrix} \tag{2}$$

The relationship between rotation matrix $\boldsymbol{C}_A^{\boldsymbol{B}}$ and $\boldsymbol{q}$ is calculated as:

$$\boldsymbol{C}_A^{\boldsymbol{B}} = (q_0^2 - \boldsymbol{q}_v^T\boldsymbol{q}_v)\boldsymbol{I}_3 + 2\boldsymbol{q}_v\boldsymbol{q}_v^T + 2q_0S(\boldsymbol{q}_v) \tag{3}$$

$$\dot{\boldsymbol{C}}_A^{\boldsymbol{B}} = -S(\boldsymbol{\omega})\boldsymbol{C}_A^{\boldsymbol{B}} \tag{4}$$

The derivative of a quaternion is given by the quaternion multiplication of the quaternion $\boldsymbol{q}$ and the angular velocity of the system $\boldsymbol{\omega}$:

$$\dot{\boldsymbol{q}} = \begin{bmatrix} \dot{q}_0 \\ \dot{\boldsymbol{q}}_v \end{bmatrix} = \frac{1}{2}\boldsymbol{q} \otimes \begin{bmatrix} 0 \\ \boldsymbol{\omega} \end{bmatrix} = \frac{1}{2}\begin{bmatrix} -\boldsymbol{q}_v^T \\ S(\boldsymbol{q}_v) + q_0\boldsymbol{I}_3 \end{bmatrix}\boldsymbol{\omega} \tag{5}$$

The quaternion error $\boldsymbol{q_e}$ is given as the quaternion multiplication of the conjugate of the actual quaternion $\boldsymbol{q}$ and the desired quaternion $\boldsymbol{q_d}$:

$$\boldsymbol{q_e} = \boldsymbol{q_d^*} \otimes \boldsymbol{q} = \begin{bmatrix} q_{0e} \\ \boldsymbol{q_{ve}} \end{bmatrix} = \begin{bmatrix} q_0 q_{0d} + \boldsymbol{q_v^T q_{vd}} \\ q_{0d}\boldsymbol{q_v} - q_0 \boldsymbol{q_{vd}} + S(\boldsymbol{q_v})\boldsymbol{q_{vd}} \end{bmatrix} \tag{6}$$

III. MATHEMATICAL MODEL AND PROBLEM FORMULATION

A. KINEMATICS AND DYNAMICS OF QUADROTOR

In this section, the kinematic and dynamic differential equations of the quadrotor are established. The quadrotor can be considered as a rigid cross frame attached with four rotors, and the center of gravity coincides with the body-fixed frame origin. The simplified model of the quadrotor is presented in Figure 1, rotors $R1$ and $R3$ rotate counterclockwise, and rotors $R2$ and $R4$ rotate clockwise, each propeller rotates at the angular speed Ω_i and produces a force F_i ($i = 1, 2, 3, 4$) along the negative z-direction relative to the body frame [34], [35]:

$$F_i = -k_T \Omega_i^2 \tag{7}$$

where $k_T > 0$ denotes the aerodynamic coefficient which consists formed of the atmospheric density ρ, the radius of the propeller r, and the thrust coefficient c_T. In addition, due to the spinning of the rotors, a reaction torque M_i ($i = 1, 2, 3, 4$) is generated on the quadrotor body by each rotor:

$$M_i = (-1)^{i+1} k_D \Omega_i^2 \tag{8}$$

where $k_D > 0$ denotes the drag coefficient of the rotor, which depends on the same factors as k_T.

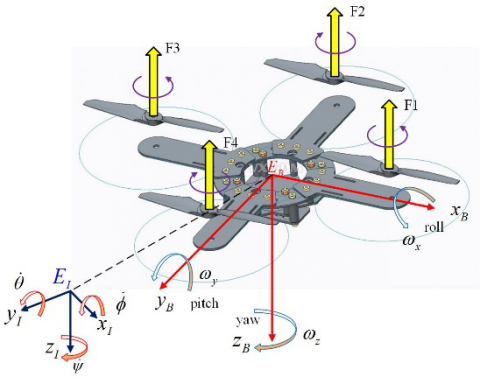

FIGURE 1. Coordinate systems of the quadrotor.

In the mathematical model of quadrotor, three coordinate frames are considered: the non-moving inertial frame E_I : $\{o_I, x_I, y_I, z_I\}$, the body-fixed frame E_B : $\{o_B, x_B, y_B, z_B\}$ and the desired frame E_D : $\{o_D, x_D, y_D, z_D\}$ to represent the actual attitude and desired attitude of quadrotor respectively. Note that NED coordinates are used to define all frames. Attitude angle and angular velocities of the body-fixed frame E_B with respect to the inertial frame E_I are written as $\Theta = [\,\phi\ \theta\ \psi\,]^T$ and $\boldsymbol{\omega} = [\,\omega_x\ \omega_y\ \omega_z\,]^T$ respectively, and the quaternion expression of the attitude is $\boldsymbol{q} = [\,q_0\ \boldsymbol{q_v}\,]^T$.

The variation of the orientation is achieved by varying the angular speed of a specific rotor. The torque created around a particular axis with respect to the body-fixed frame is defined as follows:

$$\boldsymbol{u} = \begin{bmatrix} \tau_\phi \\ \tau_\theta \\ \tau_\psi \end{bmatrix} = \begin{bmatrix} 0 & -lk_T & 0 & lk_T \\ lk_T & 0 & -lk_T & 0 \\ -k_D & k_D & -k_D & k_D \end{bmatrix} \begin{bmatrix} \Omega_1^2 \\ \Omega_2^2 \\ \Omega_3^2 \\ \Omega_4^2 \end{bmatrix} \tag{9}$$

where $\boldsymbol{u}$ represents the control signal to be designed.

Assuming a symmetric mass distribution of the quadrotor, the nominal inertia matrix $\boldsymbol{J} = \mathrm{diag}(J_x, J_y, J_z)$ is diagonal, and there exist some errors between actual inertia and $\boldsymbol{J}$. With the disturbances $\boldsymbol{d} = [\,d_x\ d_y\ d_z\,]^T$ into consideration, the attitude dynamic model of the quadrotor can be obtained as the following differential equations:

$$\begin{bmatrix} J_x\dot{\omega}_x \\ J_y\dot{\omega}_y \\ J_z\dot{\omega}_z \end{bmatrix} + \begin{bmatrix} (J_z - J_y)\omega_y\omega_z \\ (J_x - J_z)\omega_x\omega_z \\ (J_y - J_z)\omega_x\omega_y \end{bmatrix} = \begin{bmatrix} \tau_\phi \\ \tau_\theta \\ \tau_\psi \end{bmatrix} + \begin{bmatrix} d_x \\ d_y \\ d_z \end{bmatrix} \tag{10}$$

According to (6), we summarized the mathematical model of the quadrotor as:

$$\begin{cases} \dot{\boldsymbol{q}} = \dfrac{1}{2}\boldsymbol{q} \otimes [0 \quad \boldsymbol{\omega}]^T \\ \dot{\boldsymbol{\omega}} = -\boldsymbol{J}^{-1} S(\boldsymbol{\omega})\boldsymbol{J}\boldsymbol{\omega} + \boldsymbol{J}^{-1}\boldsymbol{u} + \boldsymbol{J}^{-1}\boldsymbol{d} \end{cases} \tag{11}$$

In practice, we can use micro electro mechanical system (MEMS) inertial measurement unit (IMU) to measure the attitude information $\boldsymbol{\omega}$ and $\boldsymbol{q}$.

B. DISTURBANCES

In this article, a Dryden wind gust model is introduced to the system [36]. We assume that the disturbance caused by wind field is proportional to the wind speed, therefore, $\boldsymbol{d_w}$ can be described based on the random theory [37] and defined as a summation of sinusoidal excitations:

$$d_{w,k}(t) = d_{w,k}^0 + \sum_{i=1}^{n_k} a_{k,i} \sin(\varpi_{k,i} t + \varphi_{k,i}) \tag{12}$$

where $d_{w,k}(t)$ is a time-dependent description of the wind disturbance in $k = \phi, \theta, \psi$ channel in a given time t. $\varpi_{k,i}$ and $\varphi_{k,i}$ are randomly selected frequencies and phase shifts, n_k is the number of sinusoids, $a_{k,i}$ is the amplitude of the sinusoid, and $d_{w,k}^0$ is the static wind disturbance.

Except for wind disturbance, there still exist some model uncertainties in the system. Among them, errors in inertia is relatively large. Define $\Delta\boldsymbol{J}$ as the errors in inertia matrix, we can obtain the disturbance as:

$$\boldsymbol{d_I} = S(\boldsymbol{\omega})\Delta\boldsymbol{J}\boldsymbol{\omega} - \Delta\boldsymbol{J}\dot{\boldsymbol{\omega}} \tag{13}$$

In summary, we can see that the disturbances acting on quadrotor are high-order, non-Gaussian, furthermore, their randomness and nonlinearity are very strong.

C. PROBLEM FORMULATION

In order to study the transient and steady-state characteristics of the quadrotor, the dynamics of attitude error are introduced. We use $\boldsymbol{\omega}_d = [\,\omega_{d,x}\ \omega_{d,y}\ \omega_{d,z}\,]^T$ and $\boldsymbol{q}_d = [\,q_{0d}\ \boldsymbol{q}_{vd}\,]^T$ to denote the desired angular velocities and attitude respectively, thus:

$$\boldsymbol{\omega}_e = \boldsymbol{\omega} - \boldsymbol{C}_d^b \boldsymbol{\omega}_d \tag{14}$$

where $\boldsymbol{\omega}_e = [\,\omega_{e,x}\ \omega_{e,y}\ \omega_{e,z}\,]^T$ is the tracking error vector of the angular velocities. Then, we can obtain the dynamics of $\boldsymbol{\omega}_e$ according to (4), (11), and (14):

$$\dot{\boldsymbol{\omega}}_e = S(\boldsymbol{\omega}_e)\boldsymbol{C}_d^b\boldsymbol{\omega}_d - \boldsymbol{C}_d^b\dot{\boldsymbol{\omega}}_d - \boldsymbol{J}^{-1}S(\boldsymbol{\omega})\boldsymbol{J}\boldsymbol{\omega} + \boldsymbol{J}^{-1}\boldsymbol{u} + \boldsymbol{J}^{-1}\boldsymbol{d} \tag{15}$$

where $\boldsymbol{C}_d^b$ can be calculated according to (3) and (6). And according to (5), (6), and (14), we can obtain the kinematics of attitude tracking error:

$$\dot{\boldsymbol{q}}_e = \frac{1}{2}\boldsymbol{q}_e \otimes \begin{bmatrix} 0 & \boldsymbol{\omega}_e \end{bmatrix}^T = \frac{1}{2}\begin{bmatrix} -\boldsymbol{q}_{ve}^T \\ S(\boldsymbol{q}_{ve}) + q_{0e}\boldsymbol{I}_3 \end{bmatrix}\boldsymbol{\omega}_e \tag{16}$$

The problem we try to tackle in this work is to design a continuous control law $\boldsymbol{u}$ using only the measurable system output $\boldsymbol{\omega}$ and $\boldsymbol{q}$ such that the error of attitude $\boldsymbol{\omega}_e$ (15) and $\boldsymbol{q}_e$ (16) converge to zero in presence of the disturbance. In order to achieve the high precision attitude tracking result, the DUEA strategy is necessary.

Figure 2 illustrates the control structure that we designed. Based on the DUEA control methodology, the attitude tracking problem for quadrotor can be divided into two components: design the feedforward loop so that the unmeasurable disturbances are estimated by GESO and compensated this way; and design the feedback loop that regulates the orientation to track the desired attitude produced by the commander timely. Therefore, the control signal $\boldsymbol{u}$ contains two parts as:

$$\boldsymbol{u} = \boldsymbol{u}^N + \boldsymbol{u}^E \tag{17}$$

where $\boldsymbol{u}^N$ is the nominal control input vector and $\boldsymbol{u}^E$ is the disturbances attenuation input vector.

IV. DESIGN AND ANALYSIS OF GESO

In this section, the design of GESO, which provides the disturbance estimate for the controller, is described in detail. As for the DUEA control methodology, the control performance of closed loop system will be largely determined by the observation performance. However, the disturbances acting on quadrotor are time varying, which cannot be accurately estimated by traditional ESO thoroughly [31]. So in order to enhance the performance of feedback controller, a GESO is designed to estimate the unmeasurable disturbances, and the performance analysis is carried out afterwards.

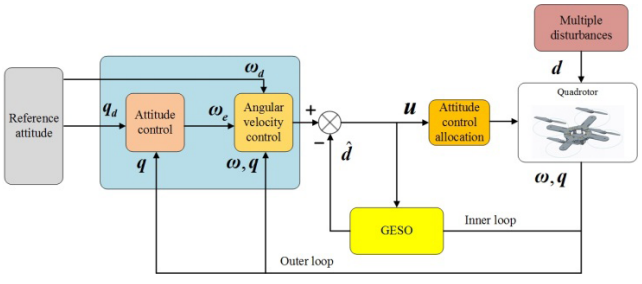

FIGURE 2. Block diagram of the proposed control scheme.

A. DESIGN OF GESO

According to the analysis of the disturbances in previous section, we can conclude that the accurate model of $\boldsymbol{d}$ is difficult to obtain in this application. In which case, we generally approximate $\boldsymbol{d}$ as a form of time polynomials [38] such as:

$$\boldsymbol{d} = \boldsymbol{b}_0 + \boldsymbol{b}_1 t + \boldsymbol{b}_2 t^2 + \cdots + \boldsymbol{b}_{n-1}t^{n-1} + \Delta(t) \tag{18}$$

where $\boldsymbol{b}_i \in \mathbb{R}^3$, $i \in \{0, 1, 2, \ldots, n-1\}$ are constant coefficients, the values of which are unknown, $\Delta(t)$ represents the residual error. Suppose that the $(n-1)$-order derivative of $\boldsymbol{d}$ is a Lipschitz continuous time signal with a known Lipschitz constant L_i, *i.e.* $\left|d_i^{(n)}\right| < L_i$, $(i = x, y, z)$. So that we can extend the variables $\boldsymbol{d}, \boldsymbol{d}^{(1)}, \ldots, \boldsymbol{d}^{n-1}$ as states of the observer:

$$\boldsymbol{\xi} = [\boldsymbol{d} \quad \boldsymbol{d}^{(1)} \quad \cdots \quad \boldsymbol{d}^{(n-1)}]^T \tag{19}$$

Consider the dynamics equations of quadrotor (10), as the angular velocities $\boldsymbol{\omega}$ can be measured by the MEMS gyroscope, feedback linearization method is introduced so that the nonlinear part of the control system can be compensated by the input $\boldsymbol{u} = \boldsymbol{u}^* + S(\boldsymbol{\omega})\boldsymbol{J}\boldsymbol{\omega}$. Therefore, the linearized model of the quadrotor is given by $\boldsymbol{J}\dot{\boldsymbol{\omega}} = \boldsymbol{u}^* + \boldsymbol{d}$, it can be written in the form of a state space system:

$$\dot{\boldsymbol{x}}_0 = \boldsymbol{B}_0\boldsymbol{u}^* + \boldsymbol{B}_{0d}\boldsymbol{d} \tag{20}$$

where $\boldsymbol{B}_0 = \boldsymbol{B}_{0d} = \boldsymbol{I}$. Define $\boldsymbol{x} = [\,(\boldsymbol{J}\dot{\boldsymbol{\omega}})^T\ \boldsymbol{\xi}^T\,]^T$ as the new state vector, the augmented system can be written as:

$$\begin{cases} \dot{\boldsymbol{x}} = \boldsymbol{A}\boldsymbol{x} + \boldsymbol{B}_d\boldsymbol{d}^{(n)} + \boldsymbol{B}\boldsymbol{u}^* \\ \boldsymbol{y} = \boldsymbol{C}\boldsymbol{x} \end{cases} \tag{21}$$

where

$$\boldsymbol{A} = \begin{bmatrix} \boldsymbol{0}_3 & \boldsymbol{I}_3 & \cdots & \boldsymbol{0}_3 & \boldsymbol{0}_3 \\ & \boldsymbol{0}_3 & \cdots & \boldsymbol{0}_3 & \boldsymbol{0}_3 \\ & & \ddots & \vdots & \vdots \\ & & & \boldsymbol{0}_3 & \boldsymbol{I}_3 \\ & & & & \boldsymbol{0}_3 \end{bmatrix}, \quad \boldsymbol{B} = \begin{bmatrix} \boldsymbol{I}_3 \\ \boldsymbol{0}_3 \\ \vdots \\ \boldsymbol{0}_3 \\ \boldsymbol{0}_3 \end{bmatrix},$$

$$\boldsymbol{B}_d = \begin{bmatrix} \boldsymbol{0}_3 \\ \boldsymbol{0}_3 \\ \vdots \\ \boldsymbol{0}_3 \\ \boldsymbol{I}_3 \end{bmatrix}, \quad \boldsymbol{C} = \begin{bmatrix} \boldsymbol{I}_3 \\ \boldsymbol{0}_3 \\ \vdots \\ \boldsymbol{0}_3 \\ \boldsymbol{0}_3 \end{bmatrix}, \quad \boldsymbol{A} \in \mathbb{R}^{3(n+1)\times 3(n+1)};$$

$\boldsymbol{B}, \boldsymbol{B}_d, \boldsymbol{C} \in \mathbb{R}^{3(n+1)\times 3}$, $\boldsymbol{I}_3$ and $\boldsymbol{0}_3$ denote identity and zero matrices with dimensions of 3×3 respectively.

Note that in the augmented model of quadrotor, it can be verified that the pair $(\boldsymbol{A}, \boldsymbol{C})$ is observable. Then, consider $\hat{\boldsymbol{x}}$ as the estimate of $\boldsymbol{x}$, $\hat{\boldsymbol{y}} = \boldsymbol{C}\hat{\boldsymbol{x}}$ as the estimate of the output $\boldsymbol{y}$, GESO can be designed as follows:

$$\begin{cases} \dot{\hat{\boldsymbol{x}}} = \boldsymbol{A}\hat{\boldsymbol{x}} + \boldsymbol{B}\boldsymbol{u}^* + \boldsymbol{L}\boldsymbol{C}\left(\boldsymbol{x} - \hat{\boldsymbol{x}}\right) \\ \hat{\boldsymbol{y}} = \boldsymbol{C}\hat{\boldsymbol{x}} \end{cases} \tag{22}$$

where $\boldsymbol{L} = [l_0\boldsymbol{I}_3 \; l_1\boldsymbol{I}_3 \; l_2\boldsymbol{I}_3 \; \cdots \; l_n\boldsymbol{I}_3]^T$ is the observer gain matrices to be designed.

Define the estimation errors as $\tilde{\boldsymbol{x}} = \boldsymbol{x} - \hat{\boldsymbol{x}}$, we get the following error dynamics:

$$\dot{\tilde{\boldsymbol{x}}} = (\boldsymbol{A} - \boldsymbol{L}\boldsymbol{C})\tilde{\boldsymbol{x}} + \boldsymbol{B}_{\boldsymbol{d}}\boldsymbol{d}^{(n)} \tag{23}$$

B. STABILITY ANALYSIS OF GESO

Define the Lyapunov candidate function V_0 as:

$$V_0 = \tilde{\boldsymbol{x}}^T\boldsymbol{P}\tilde{\boldsymbol{x}} \tag{24}$$

Its time derivative is written as:

$$\dot{V}_0 = \tilde{\boldsymbol{x}}^T((\boldsymbol{A} - \boldsymbol{L}\boldsymbol{C})^T\boldsymbol{P} + \boldsymbol{P}(\boldsymbol{A} - \boldsymbol{L}\boldsymbol{C}))\tilde{\boldsymbol{x}} + 2\tilde{\boldsymbol{x}}^T\boldsymbol{P}\boldsymbol{B}_{\boldsymbol{d}}\boldsymbol{d}^{(n)} \tag{25}$$

Consider the time derivative of V_0. Under the condition that $\boldsymbol{A} - \boldsymbol{L}\boldsymbol{C}$ is Hurwitz and for any $k_0 > 0$, there exists a positive definite symmetric matrix $\boldsymbol{P}$ satisfying:

$$(\boldsymbol{A} - \boldsymbol{L}\boldsymbol{C})^T\boldsymbol{P} + \boldsymbol{P}(\boldsymbol{A} - \boldsymbol{L}\boldsymbol{C}) = -k_0\boldsymbol{I}_3 \tag{26}$$

Substituting (26) into (25), we can get:

$$\begin{aligned} \dot{V}_0 &= -k_0\tilde{\boldsymbol{x}}^T\tilde{\boldsymbol{x}} + 2\tilde{\boldsymbol{x}}^T\boldsymbol{P}\boldsymbol{B}_{\boldsymbol{d}}\boldsymbol{d}^{(n)} \\ &\leq -\|\tilde{\boldsymbol{x}}\|\left(\|\tilde{\boldsymbol{x}}\|k_0 - 2\|\boldsymbol{P}\boldsymbol{B}_{\boldsymbol{d}}\|\left\|\boldsymbol{d}^{(n)}\right\|\right) \\ &\leq -\|\tilde{\boldsymbol{x}}\|\left(\|\tilde{\boldsymbol{x}}\|k_0 - 2\gamma\lambda_1\right) \end{aligned} \tag{27}$$

where $\boldsymbol{d}^{(n)}$ is bounded with $\left\|\boldsymbol{d}^{(n)}\right\| \leq \sqrt{L_x^2 + L_y^2 + L_z^3} = \gamma$, and λ_1 is the 2-norm of $\|\boldsymbol{P}\boldsymbol{B}_{\boldsymbol{d}}\|$. It is obvious that $\dot{\boldsymbol{V}}_0 < 0$ whenever $\|\tilde{\boldsymbol{x}}\| > 2\gamma\lambda_1k_0^{-1}$. Therefore, the upper bound for estimation error $\|\tilde{\boldsymbol{x}}\|$ will be constrained by the bounded ball $B_r = \left\{\boldsymbol{r} \middle| \|\boldsymbol{r}\| \leq 2\gamma\lambda_1k_0^{-1}\right\}$ and the disturbances attenuation inputs $\boldsymbol{u}^{\boldsymbol{E}}$ can be select as:

$$\boldsymbol{u}^{\boldsymbol{E}} = -\hat{\boldsymbol{\xi}}_{\boldsymbol{1}} \tag{28}$$

C. GAIN TUNING GUIDELINES FOR GESO

In this section, we use frequency response analysis to discuss the gain tuning guidelines of GESO [30], [39]. To this end, the relationship between $\boldsymbol{d}$ and $\tilde{\boldsymbol{d}}$ should be obtained. According to (23), we have:

$$\tilde{\boldsymbol{d}} = \dot{\tilde{\boldsymbol{x}}}_0 + l_0\tilde{\boldsymbol{x}}_0 \tag{29}$$

$$\boldsymbol{d}^{(n)} = l_n\tilde{\boldsymbol{x}}_0 + l_{n-1}\dot{\tilde{\boldsymbol{x}}}_0 + \cdots + l_0\tilde{\boldsymbol{x}}_0^{(n)} + \tilde{\boldsymbol{x}}_0^{(n+1)} \tag{30}$$

where $\tilde{\boldsymbol{d}} = \tilde{\boldsymbol{\xi}}_1$ is the disturbance estimation error. Under zero initial condition, the s-domain expressions of the former equation are:

$$\tilde{\boldsymbol{d}} = s\tilde{\boldsymbol{x}}_0 + l_0\tilde{\boldsymbol{x}}_0 \tag{31}$$

$$s^n\boldsymbol{d} = \left(s^{n+1} + l_0s^n + \cdots + l_n\right)\tilde{\boldsymbol{x}}_0 \tag{32}$$

We can get relationship between the estimation error of the disturbance $\tilde{\boldsymbol{d}}$ and the disturbance input $\boldsymbol{d}$ according to the former equation:

$$\tilde{\boldsymbol{d}}(s) = \frac{s^n(s + l_0)}{s^{n+1} + l_0s^n + l_1s^{n-1} + \cdots + l_n}\boldsymbol{d} = G(s)\boldsymbol{d}(s) \tag{33}$$

From (33), we can conclude that for a given input of disturbances $\boldsymbol{d}$, the response of estimation error $\tilde{\boldsymbol{d}}$ depends on the observer gains $l_0, l_1, \ldots, l_n$. Once the bandwidth ω_b and the order n are chosen, we can obtain the observer gains by evaluating:

$$s^{n+1} + l_0s^n + l_1s^{n-1} + \cdots + l_{n-1}s + l_n = (s + \omega_b)^{n+1} \tag{34}$$

Thus, the observer gain $\boldsymbol{L} = [l_0\boldsymbol{I}_3 \; l_1\boldsymbol{I}_3 \; l_2\boldsymbol{I}_3 \; \cdots \; l_n\boldsymbol{I}_3]^T$ is calculated as:

$$\begin{cases} l_0 = C_{n+1}^1\omega_b \\ \quad\vdots \\ l_i = C_{n+1}^{i+1}\omega_b^{i+1} \\ \quad\vdots \\ l_n = C_{n+1}^{n+1}\omega_b^{n+1} \end{cases} \tag{35}$$

Then, we study the influence of the observer bandwidth ω_b and the order of GESO n on the estimation accuracy of GESO [30]. For a given ω_b and n, $G(s)$ can be written as:

$$G(s) = \frac{s^n(s + (n+1)\omega_b)}{(s + \omega_b)^{n+1}} \tag{36}$$

The frequency response of (36) is analyzed. In Fig.3 (a), the magnitude plots for the first-, second-, and third-order GESO are shown when the bandwidth of GESO ω_b is fixed at 20rad/s. It can be seen that as the order of the ESO increases, the attenuation for the low-frequency components improves, resulting in reduction in the disturbance estimation error. In Fig.3 (b), the magnitude plots for the third-order GESO are shown on condition that the bandwidths ω_b of GESO are chosen as 10rad/s 20rad/s and 40rad/s respectively. It is obvious that for a given order of the GESO, the attenuation for the low-frequency components improves as the bandwidth of GESO is increased, thus the estimation accuracy of multiple disturbances is increased.

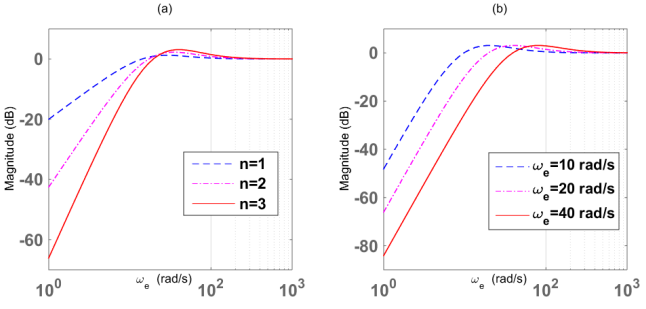

FIGURE 3. Bode plots for G(s); (a) Different order with fixed bandwidth ω_b = 20rad/s; (b) Different bandwidth with fixed order n = 3.

The expressions for magnitudes of $G(s)$ can be obtained as:

$$|G(j\omega)| = \kappa^n \sqrt{\frac{\kappa^2 + (n+1)^2}{\left(\kappa^2+1\right)^{n+1}}} \tag{37}$$

where $\kappa = \omega_b^{-1}\omega$ and if $\omega \ll \omega_b$, (37) can be simplified as:

$$|G(j\omega)| \approx (n+1)\,\kappa^n \tag{38}$$

From (38), we can conclude that as n and ω_b increases, the peak magnitudes of $G(s)$ decreases. But a larger GESO order can also increase the computational burden, and a larger bandwidth will also lead to a larger observer gain, which in turn amplifies the effect of sensor noise. Therefore, the choice of n and ω_b is a compromise between the estimation accuracy and computational efficiency.

V. DESIGN OF ATTITUDE TRACKING CONTROLLER

In this section, the main procedures of attitude tracking controller integrated with GESO are presented for effectively handling disturbances existed in the quadrotor to achieve highly precise attitude tracking. The quadrotor UAV is an underactuated system with six DOF and four control inputs. In order to derive its model, backstepping method is used in the design of attitude tracking controller.

Step 1: Design the control strategy to ensure that $\boldsymbol{q_e}(t)$ converges to zero.

According to the attitude error kinematics subsystem (16), we select the candidate Lyapunov function as:

$$V_1 = \boldsymbol{q_e}^T\boldsymbol{q_e} + (1-q_{0e})^2 > 0 \tag{39}$$

Take the time derivative of V_1:

$$\begin{aligned}\dot{V}_1 &= 2\boldsymbol{q_{ve}}^T\dot{\boldsymbol{q}}_{\boldsymbol{ve}} - 2(1-q_{0e})\dot{q}_{0e}\\ &= (\boldsymbol{q_{ve}}^T S(\boldsymbol{q_{ve}}) + q_{0e}\boldsymbol{q_{ve}}^T\boldsymbol{I}_3 + (1-q_{0e})\boldsymbol{q_{ve}}^T)\boldsymbol{\omega_e}\\ &= \boldsymbol{q_{ve}}^T\boldsymbol{\omega_e}\end{aligned} \tag{40}$$

Then we design a virtual control scheme as:

$$\boldsymbol{\omega}_{ed} = -\boldsymbol{K}_1\boldsymbol{q}_e \tag{41}$$

where $\boldsymbol{K}_1$ is the gain matrix of the controller, which is diagonal positive definite. If the angular velocity tracking error $\boldsymbol{\omega}_e$ is equal to the virtual control input $\boldsymbol{\omega}_{ed}$, $\dot{V}_1$ is negative semidefinite definite:

$$\dot{V}_1 = -\boldsymbol{q}_e^T\boldsymbol{K}_1\boldsymbol{q}_e \tag{42}$$

According to the Lyapunov stability theorem, we can conclude that $\boldsymbol{q_e}$ converges to zero, under the condition that the virtual control $\boldsymbol{\omega}_e$ converges to $-\boldsymbol{K}_1\boldsymbol{q}_e$.

Step 2: Design the control signal $\boldsymbol{u}$ to ensure that $\boldsymbol{\omega}_e$ track the desired virtual control input $\boldsymbol{\omega}_{ed}$.

We define the error between $\boldsymbol{\omega_e}$ and $\boldsymbol{\omega}_{ed}$ as:

$$\tilde{\boldsymbol{\omega}}_{\boldsymbol{e}} = \boldsymbol{\omega_e} + \boldsymbol{K}_1\boldsymbol{q_e} \tag{43}$$

In order to discuss the stability of the entire system including DUE and FC, we define the following candidate Lyapunov function V_2 as:

$$\begin{aligned}V_2 &= V_0 + V_1 + \frac{1}{2}\tilde{\boldsymbol{\omega}}_{\boldsymbol{e}}^T\boldsymbol{J}\tilde{\boldsymbol{\omega}}_{\boldsymbol{e}}\\ &= \left[\boldsymbol{q}_{\boldsymbol{e}}^T\boldsymbol{q_e} + (1-q_{0e})^2\right] + \frac{1}{2}\tilde{\boldsymbol{\omega}}_{\boldsymbol{e}}^T\boldsymbol{J}\tilde{\boldsymbol{\omega}}_{\boldsymbol{e}} + \tilde{\boldsymbol{x}}^T\boldsymbol{P}\tilde{\boldsymbol{x}}\end{aligned} \tag{44}$$

Take the time derivative of V_2, and substitute (15), (40), and (42) into $\dot{V}_2$:

$$\begin{aligned}\dot{V}_2 &= \boldsymbol{q_{ve}}^T\tilde{\boldsymbol{\omega}}_{\boldsymbol{e}} - \boldsymbol{q_{ve}}^T\boldsymbol{K}_1\boldsymbol{q_{ve}} + \tilde{\boldsymbol{\omega}}_{\boldsymbol{e}}^T(\boldsymbol{J}\dot{\boldsymbol{\omega}}_{\boldsymbol{e}} + \boldsymbol{J}\boldsymbol{K}_1\dot{\boldsymbol{q}}_{\boldsymbol{ve}}) + \dot{V}_0\\ &= -\boldsymbol{q_{ve}}^T\boldsymbol{K}_1\boldsymbol{q_{ve}} + \tilde{\boldsymbol{\omega}}_{\boldsymbol{e}}^T(\boldsymbol{u} + \boldsymbol{d} + \mathbb{N}) + \dot{V}_0\end{aligned} \tag{45}$$

where $\mathbb{N} = \boldsymbol{J}(S(\boldsymbol{\omega_e})\boldsymbol{C}_{\boldsymbol{d}}^{\boldsymbol{b}}\boldsymbol{\omega_d} - \boldsymbol{C}_{\boldsymbol{d}}^{\boldsymbol{b}}\dot{\boldsymbol{\omega}}_{\boldsymbol{d}}) - S(\boldsymbol{\omega})\boldsymbol{J}\boldsymbol{\omega} + \boldsymbol{J}\boldsymbol{K}_1\dot{\boldsymbol{q}}_{\boldsymbol{ve}} + \boldsymbol{q_{ve}}$. We define $\boldsymbol{u}^{\boldsymbol{N}} = -\mathbb{N} - \boldsymbol{K}_2\tilde{\boldsymbol{\omega}}_{\boldsymbol{e}}$, and plug (27) and (28) into (45):

$$\begin{aligned}\dot{V}_2 &= -\boldsymbol{q_{ve}}^T\boldsymbol{K}_1\boldsymbol{q_{ve}} - k_0\tilde{\boldsymbol{x}}^T\tilde{\boldsymbol{x}} - \tilde{\boldsymbol{\omega}}_{\boldsymbol{e}}^T\boldsymbol{K}_2\tilde{\boldsymbol{\omega}}_{\boldsymbol{e}} + \tilde{\boldsymbol{\omega}}_{\boldsymbol{e}}^T\tilde{\boldsymbol{d}} + 2\tilde{\boldsymbol{x}}^T\boldsymbol{P}\boldsymbol{B}_{\boldsymbol{d}}\boldsymbol{d}^{(n)}\\ &\le -\lambda_2\left\|\boldsymbol{q_{ve}}\right\|^2 - \lambda_3\left\|\tilde{\boldsymbol{\omega}}_{\boldsymbol{e}}\right\|^2 - k_0\left\|\tilde{\boldsymbol{x}}\right\|^2 + \left\|\tilde{\boldsymbol{\omega}}_{\boldsymbol{e}}\right\|\left\|\tilde{\boldsymbol{d}}\right\|\\ &\quad + 2\lambda_1\gamma\left\|\tilde{\boldsymbol{x}}\right\|\\ &\le -\lambda_2\left\|\boldsymbol{q_{ve}}\right\|^2 - \lambda_3\left\|\tilde{\boldsymbol{\omega}}_{\boldsymbol{e}}\right\|^2 - k_0\left\|\tilde{\boldsymbol{x}}\right\|^2 + \left\|\tilde{\boldsymbol{\omega}}_{\boldsymbol{e}}\right\|\left\|\tilde{\boldsymbol{x}}\right\|\\ &\quad + 2\lambda_1\gamma\left\|\tilde{\boldsymbol{x}}\right\|\\ &\le -\lambda_2\left\|\boldsymbol{q_{ve}}\right\|^2 - \left(\lambda_3 - \frac{1}{2}\right)\left\|\tilde{\boldsymbol{\omega}}_{\boldsymbol{e}}\right\|^2 - \left(k_0 - \frac{1}{2}\right)\left\|\tilde{\boldsymbol{x}}\right\|^2\\ &\quad + 2\lambda_1\gamma\left\|\tilde{\boldsymbol{x}}\right\|\end{aligned} \tag{46}$$

where $\left\|\tilde{\boldsymbol{d}}\right\| = \left\|\tilde{\boldsymbol{\xi}}_1\right\| \le \|\tilde{\boldsymbol{x}}\|$, λ_2 and λ_3 are the minimal eigenvalue of $\boldsymbol{K}_1$ and $\boldsymbol{K}_2$ respectively. Define $\boldsymbol{z}^T = (\boldsymbol{q}_{\boldsymbol{e}}^T, \tilde{\boldsymbol{\omega}}_{\boldsymbol{e}}^T, \tilde{\boldsymbol{x}}^T)$ as the uniformed vector of errors, and $\eta = \min(\lambda_2, \lambda_3 - \frac{1}{2}, k_0 - \frac{1}{2}) > 0$, then (46) can be reduced to:

$$\begin{aligned}\dot{V}_3 &\le -\eta\left(\left\|\boldsymbol{q_{ve}}\right\|^2 + \left\|\tilde{\boldsymbol{\omega}}_{\boldsymbol{e}}\right\|^2 + \left\|\tilde{\boldsymbol{x}}\right\|^2\right) + 2\lambda_1\gamma\left\|\tilde{\boldsymbol{x}}\right\|\\ &\le -\eta\left\|z\right\|^2 + 2\lambda_1\gamma\left\|z\right\|\end{aligned} \tag{47}$$

Thus $\dot{V}_3 < 0$ whenever $\|z\| > 2\lambda_1\gamma\eta^{-1}$. Notice that $(\boldsymbol{q_e}, \tilde{\boldsymbol{\omega}}_e)$ is a linear diffeomorphism of $(\boldsymbol{q_e}, \boldsymbol{\omega}_e)$, hence $(\boldsymbol{q_e}, \boldsymbol{\omega}_e)$ can converge into a compact set. We can conclude that, the attitude error $(\boldsymbol{q_e}, \boldsymbol{\omega}_e)$, virtual control input error $\tilde{\boldsymbol{\omega}}_e$ and the estimation error $\tilde{\boldsymbol{x}}$ are uniformly ultimately bounded and exponentially converges to the bounded ball $B_z = \left\{z \middle| \|z\| \le 2\gamma\lambda_1\eta^{-1}\right\}$.

In general, when we chose a larger η, the bounded ball B_z will become smaller and consequently, $\|z\|$ will also become smaller, so a larger η is preferred. However, larger η will lead to larger control gains which can excite the sensor noise and undesirable high frequency dynamics of the system. Thus, the tuning of controller parameters is a tradeoff between the demand of performance and the real conditions.

VI. SIMULATION AND EXPERIMENTAL RESULTS

In order to evaluate the performance of the proposed GESO with different order, simulation and real world experimental results are presented in this section. Mainly, two performance metrics are evaluated. One is the attitude tracking stability, and the other is the robustness to the disturbances.

A. SIMULATION RESULTS

We present the numerical simulations of the proposed GESO based DUEA control strategy on a model generated by the online toolbox of Quan and Dai [40], and the values are listed in Table 1.

TABLE 1. Quadrotor parameters used in simulation.

Parameter	Description	value
m	Mass	1.79 kg
Jx	Roll inertia	1.335×10^{-2} kg·m^2
Jy	Pitch inertia	1.335×10^{-2} kg·m^2
Jz	Yaw inertia	2.465×10^{-2} kg·m^2
l	Motor moment arm	0.18 m
g	Gravity acceleration	9.81 g·s^2
k_T	Aerodynamic coefficient	8.82×10^{-6} kg·m
k_D	Drag coefficient	1.09×10^{-7} kg·m^2

In numerical simulations, the errors in inertia are 30% *i.e.* $\Delta\boldsymbol{J} = 0.3\boldsymbol{J}$. According to [41], the disturbance torque caused by the wind field is proportional to the wind speed. Therefore, without loss of generality, it can be assumed that the three-axis components of $\boldsymbol{d_w} = [\,d_{w,\phi}\ d_{w,\theta}\ d_{w,\psi}\,]^T$ are equal $d_{w,\phi} = d_{w,\theta} = d_{w,\psi} = d_w$. The values of $\varpi_{k,i}$ are taken between 0.05π rad/s and 2.5π rad/s. The disturbance torque used in numerical simulation is Eq. (48), and is visualized as Figure 4.

$$\begin{aligned} d_w = {} & \sin(2.5\pi t - 3) + 1.5\sin(2\pi t + 7) \\ & + 2\sin(0.4\pi t - 9.5) + \sin(0.2\pi t) \\ & + 0.5\sin(0.08\pi t + 1) + \sin(0.07\pi t + 1.5) \\ & + 0.5\sin(0.05\pi t + 2) + 4 \end{aligned} \tag{48}$$

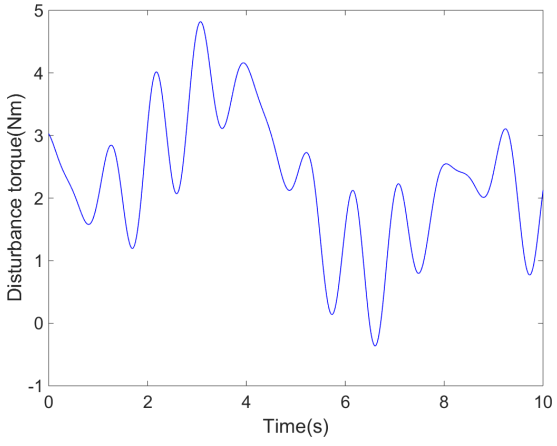

FIGURE 4. Disturbance torque applied in simulation.

The values of gain parameters used in our controller are given as $\boldsymbol{K}_1 = 11.5\boldsymbol{I}_3$ and $\boldsymbol{K}_2 = 16.2\boldsymbol{I}_3$, and the observer gains of GESO-*i* are illustrated in Table 2, where *i* is the order of GESO.

TABLE 2. Observer gains with different order.

Order	ω_b	l_0	l_1	l_2	l_3
GESO-1	20 rad/s	40	400	/	/
GESO-2	20 rad/s	60	1200	8000	/
GESO-3	20 rad/s	80	2400	32000	160000

1) CASE 1 (COMPARISON IN ATTITUDE STABILIZATION PERFORMANCE)

This part involves attitude stabilization control in the presence of disturbances. We select the desired attitude signal as follows:

$$\Theta_d = \begin{bmatrix} 30 & 15 & 25 \end{bmatrix}^T \text{ deg} \tag{49}$$

Four comparative simulations were conducted, and the performances of the proposed controller with different order GESOs are compared in each channel. Figures 5-7 show the response curves of the vehicle's attitude angles during its flight. We can see that although the proposed controller (without GESO) was able to ensure the stabilization of the attitude angles, the control accuracy was reduced under the influence of the disturbances. When we introduced GESO as the DUE, the performances of the proposed controller were improved, and the performance increases with the increase of the order of the GESO. Moreover, Figure 8 shows the disturbance estimation error of GESO with different orders. Obviously, we can see that the estimation error decreases with the increase of the observer order when the bandwidth of the GESO ω_b was fixed at 20rad/s.

2) CASE 2 (COMPARISON OF ATTITUDE TRACKING PERFORMANCE)

In this case, the numerical simulation demonstrates the effectiveness of the proposed control scheme for attitude tracking.

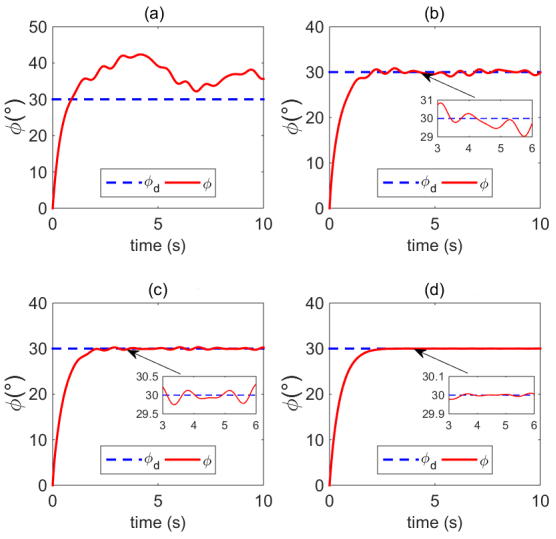

FIGURE 5. Simulation curves of Φ in Case 1. (a) Without ESO. (b) GESO-1. (c) GESO-2. (d) GESO-3.

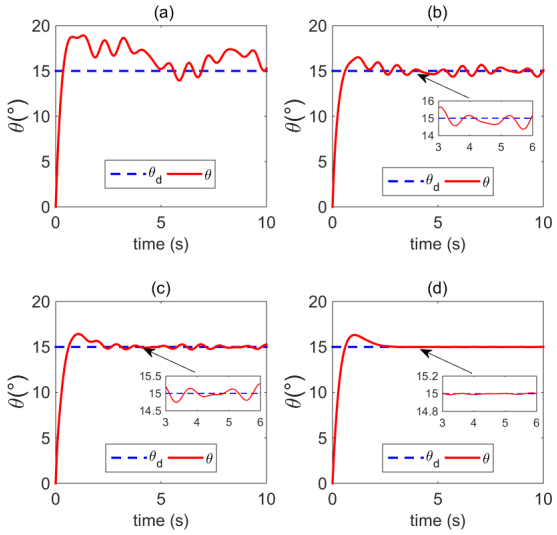

FIGURE 6. Simulation curves of θ in Case 1. (a) Without ESO. (b) GESO-1. (c) GESO-2. (d) GESO-3.

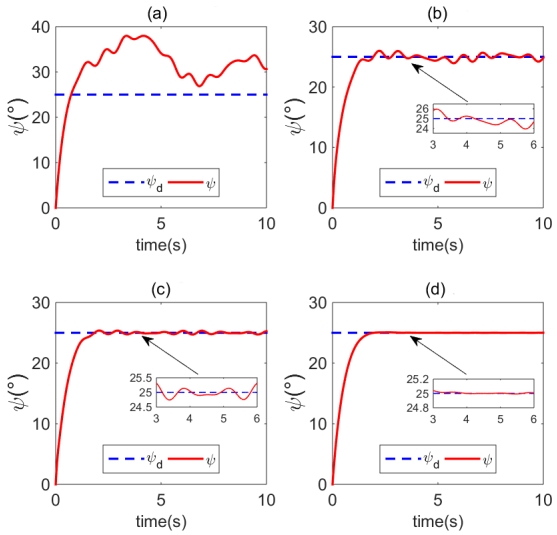

FIGURE 7. Simulation curves of ψ in Case 1. (a) Without ESO. (b) GESO-1. (c) GESO-2. (d) GESO-3.

We chose desired attitude signal as follows:

$$\Theta_d = \begin{bmatrix} \phi_d \\ \theta_d \\ \psi_d \end{bmatrix} = \begin{bmatrix} 15\sin(0.4\pi t) \\ 15\sin(0.4\pi t + 0.5\pi) \\ 25\sin(0.4\pi t + 0.25\pi) \end{bmatrix} \text{deg} \quad (50)$$

The attitude tracking performances of the proposed controller with different order GESOs are illustrated in Figures 9-11. We can see that although the proposed controller alone was able to ensure the tracking of the desired attitude angles, the control accuracy was reduced under the influence of the disturbances. When we introduced GESO as the DUE, the performances of the proposed controller were improved, and the simulation results show that with the increase of the observer order, the speed of convergence and the tracking accuracy are improved.

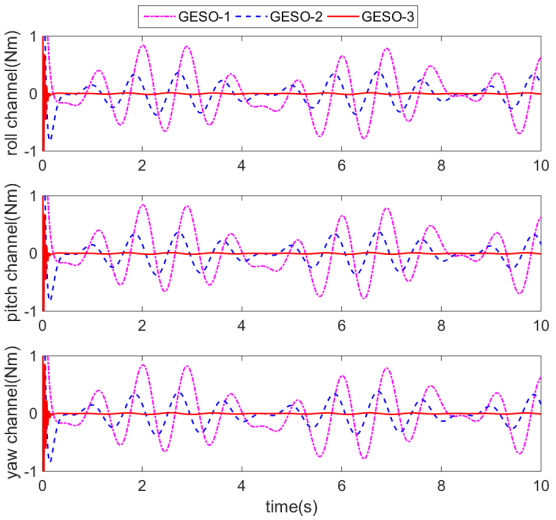

FIGURE 8. Disturbance estimation error of GESO with different order in case 1.

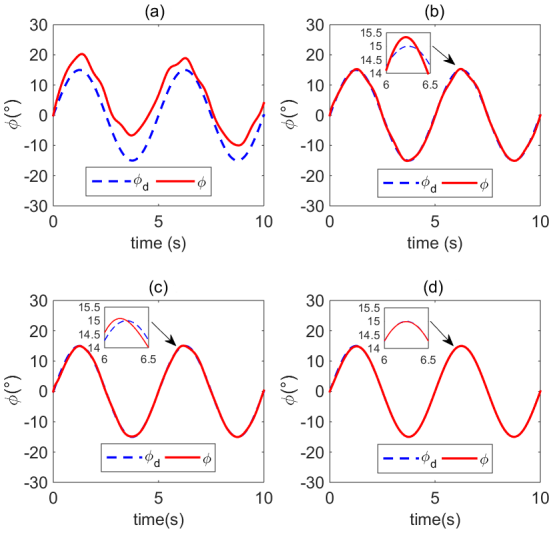

FIGURE 9. Simulation curves of Φ in Case 2. (a) Without ESO. (b) GESO-1. (c) GESO-2. (d) GESO-3.

Moreover, as shown in Figure 12, the accuracy of disturbances estimation increases with the observer order when the bandwidth of the GESO ω_b is fixed at 20rad/s.

B. EXPERIMENTAL RESULTS

We have also tested the proposed control scheme on a self-assembled GF360 quadrotor, and PIXHAWK [42], [43] was used as the autopilot of the quadrotor. To evaluate the stability and robustness of the proposed control scheme, the experiments were carried out as follows.

Without loss of generality, the longitudinal channel of the system was analyzed. Since the actual aircraft is a discrete system, both sampling frequency and control frequency will affect the choice of bandwidth, it is difficult to calculate a precise one. Therefore, we tested the stability of the system with different observer bandwidths on condition that the

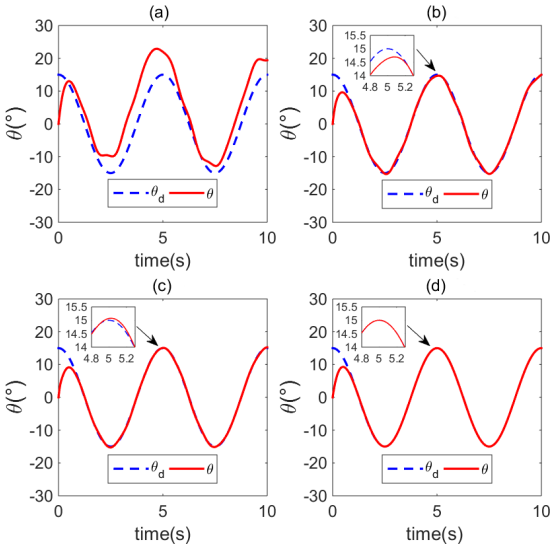

FIGURE 10. Simulation curves of θ in Case 2. (a) Without ESO. (b) GESO-1. (c) GESO-2. (d) GESO-3.

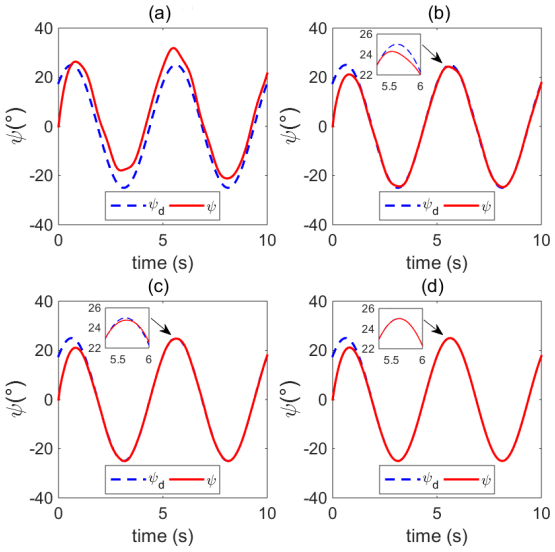

FIGURE 11. Simulation curves of ψ in Case 2. (a) Without ESO. (b) GESO-1. (c) GESO-2. (d) GESO-3.

observer order n is fixed at 3, and the experimental curves of the attitude are illustrated Figure 13.

From the experiment results, we can see that excessive bandwidth will excite the sensor noise and vibration, and then degrade the stability of the system by introducing them into the control loop. As the result, the bandwidth of GESO should not be too large. Limited by the sampling frequency and noise of MEMS IMU, we chose the bandwidth of GESO as $\omega_b = 4$rad/s based on a series of experimental tests.

Then, in order to ensure the same experimental conditions, we run our experiments in a controlled indoor environment. We used an electrical fan with adjustable wind speed to generate the disturbance torque acting on the longitudinal channel of quadrotor. The average wind speed was around 4.5 m/s. And the controller gains were chosen as

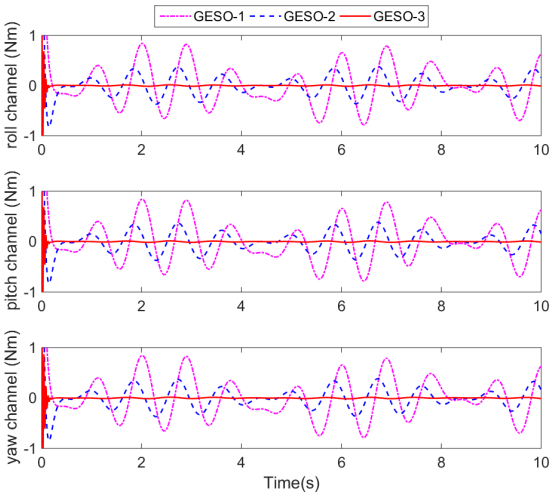

FIGURE 12. Disturbance estimation error of GESO with different order in case 2.

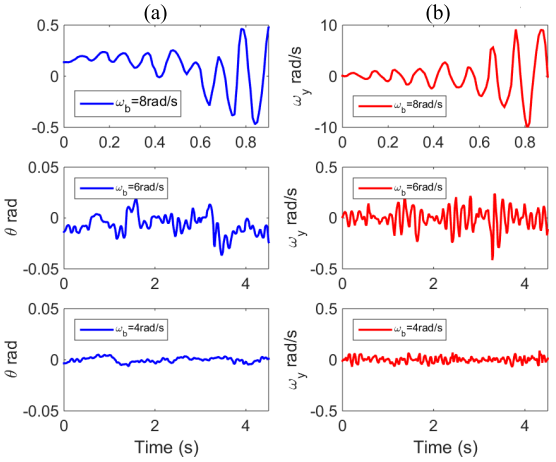

FIGURE 13. Experimental curves of the attitude with different observer bandwidths, $n = 3$. (a) Attitude angle. (b) Angular velocity.

$\boldsymbol{K}_1 = \text{diag}(7, 7, 2.8)$, $\boldsymbol{K}_2 = \text{diag}(0.15, 0.15, 0.2)$. As shown in Figure 14, the experiments were carried out in lab without GPS signals, and the quadrotor was hovering in the wind field.

Four experiments of the proposed controller with different order GESOs are presented. Figure 15 shows the experimental results of pitch rate obtained by the proposed controller with different order GESOs in the presence of wind field. And Figure 16 presents the history of pitch angle tracking errors $\theta_e = \theta - \theta_d$ in these four cases.

It can be observed that the control performance is improved by GESO compared with the one without GESO. In addition, Figure 16 shows that the tracking error of pitch angle θ_e decreases with the increase of the GESO order, and the root mean square (RMS) errors of θ_e and ω_e obtained by the proposed controller with different order GESOs are listed in Table 3. We can see that without the wind disturbance, 3rd order GESO can achieve 57.23% and 62.35% reduction

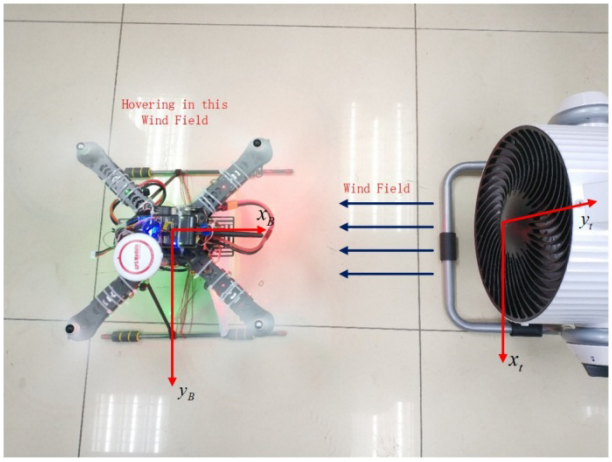

FIGURE 14. Experimental setup of the quadrotor hovering in the wind field.

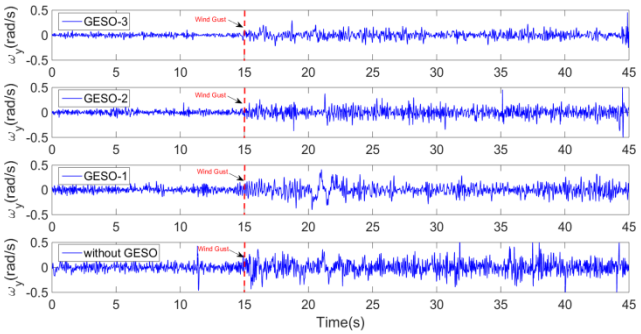

FIGURE 15. Experimental curves of ω_y with different order GESO.

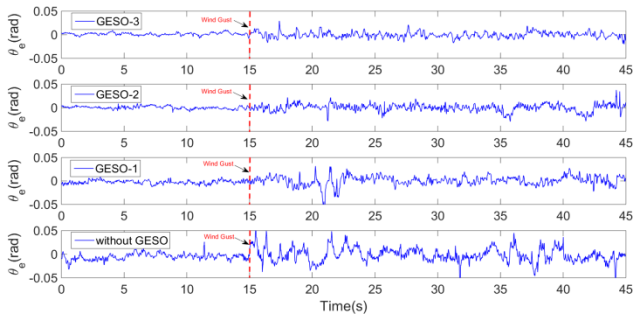

FIGURE 16. Experimental curves of θ_e with different order GESO.

on the RMS error of pitch rate and pitch angle tracking error, respectively. While with the wind disturbance, the RMS reduction is 50.38% and 60.40% reduction, respectively.

TABLE 3. Comparison of control performance with different order GESOs (RMS error).

	Without wind disturbance		With wind disturbance	
	θ_e (rad)	ω_y (rad/s)	θ_e (rad)	ω_y (rad/s)
Without GESO	0.0085	0.0685	0.0149	0.1292
GESO-*1*	0.0045	0.0490	0.0101	0.1024
GESO-*2*	0.0031	0.0365	0.0078	0.0886
GESO-*3*	0.0032	0.0293	0.0059	0.0641

VII. CONCLUSION

In this paper, the problem of high precision attitude tracking for quadrotor in the presence of disturbances is investigated. To tackle this problem, we developed a GESO based DUEA control strategy and summarized the gain tuning guidelines for GESO. From the simulation and experimental results, we can conclude that when the bandwidth of the GESO ω_b is fixed, the performance of the proposed controller improves with the increase of the GESO order. Taking the performance improvements and the computational complexity into account, we believe that the 3rd order GESO is preferred. And in the real world experiment, we chose the observer bandwidth ω_b to be 4 rad/s, mainly due to the noise and the sampling time of the MEMS IMU. Higher bandwidth of GESO can be used if the measurement noise and the sampling time of the devices are reduced, and the performance can be further improved.

REFERENCES

[1] S. Bouabdallah, M. Becker, and R. Siegwart, "Autonomous miniature flying robots: Coming soon!—Research, development, and results," *IEEE Robot. Automat. Mag.*, vol. 14, no. 3, pp. 88–98, Sep. 2007.
[2] A. C. Satici, H. Poonawala, and M. W. Spong, "Robust optimal control of quadrotor UAVs," *IEEE Access*, vol. 1, pp. 79–93, 2013.
[3] B. Tian, Y. Ma, and Q. Zong, "A continuous finite-time output feedback control scheme and its application in quadrotor UAVs," *IEEE Access*, vol. 6, pp. 19807–19813, 2018.
[4] M. J. Stepaniak, F. van Graas, and M. U. de Haag, "Design of an electric propulsion system for a quadrotor unmanned aerial vehicle," *J. Aircr.*, vol. 46, no. 3, pp. 1050–1058, May/Jun. 2009.
[5] S. Gupte, P. I. T. Mohandas, and J. M. Conrad, "A survey of quadrotor unmanned aerial vehicles," in *Proc. IEEE Southeastcon*, Mar. 2012, pp. 1–6.
[6] N. S. Özbek, M. Önkol, and M. Ö. Efe, "Feedback control strategies for quadrotor-type aerial robots: A survey," *Trans. Inst. Meas. Control*, vol. 38, no. 5, pp. 529–554, May 2016.
[7] F. Muñoz, I. González-Hernández, S. Salazar, E. S. Espinoza, and R. Lozano, "Second order sliding mode controllers for altitude control of a quadrotor UAS: Real-time implementation in outdoor environments," *Neurocomputing*, vol. 233, pp. 61–71, Apr. 2017.
[8] M. Huang, B. Xian, C. Diao, K. Yang, and Y. Feng, "Adaptive tracking control of underactuated quadrotor unmanned aerial vehicles via backstepping," in *Proc. Amer. Control Conf.*, Jun./Jul. 2010, pp. 2076–2081.
[9] D. Cabecinhas, R. Naldi, L. Marconi, C. Silvestre, and R. Cunha, "Robust take-off and landing for a quadrotor vehicle," in *Proc. IEEE Int. Conf. Robot. Automat. (ICRA)*, May 2010, pp. 1630–1635.
[10] A. L. Salih, M. Moghavvemi, H. A. F. Mohamed, and K. S. Gaeid, "Flight PID controller design for a UAV quadrotor," *Sci. Res. Essays*, vol. 5, no. 23, pp. 3660–3667, Dec. 2010.
[11] E. Reyes-Valeria, R. Enriquez-Caldera, S. Camacho-Lara, and J. Guichard, "LQR control for a quadrotor using unit quaternions: Modeling and simulation," in *Proc. 23rd Int. Conf. Electron., Commun. Comput.*, Mar. 2013, pp. 172–178.
[12] C. Nicol, C. J. B. Macnab, and A. Ramirez-Serrano, "Robust adaptive control of a quadrotor helicopter," *Mechatronics*, vol. 21, no. 6, pp. 927–938, 2011.
[13] B. Zhao, B. Xian, Y. Zhang, and X. Zhang, "Nonlinear robust sliding mode control of a quadrotor unmanned aerial vehicle based on immersion and invariance method," *Int. J. Robust Nonlinear Control*, vol. 25, no. 18, pp. 3714–3731, Dec. 2015.
[14] L. Wang and H. Jia, "The trajectory tracking problem of quadrotor UAV: Global stability analysis and control design based on the cascade theory," *Asian J. Control*, vol. 16, no. 2, pp. 574–588, 2014.
[15] Z. Gao, "On the centrality of disturbance rejection in automatic control," *ISA Trans.*, vol. 53, no. 4, pp. 850–857, 2014.
[16] W.-H. Chen, K. Ohnishi, and L. Guo, "Advances in disturbance/uncertainty estimation and attenuation," *IEEE Trans. Ind. Electron.*, vol. 62, no. 9, pp. 5758–5762, Sep. 2015.

[17] J. Yang, W.-H. Chen, S. Li, L. Guo, and Y. D. Yan, "Disturbance/uncertainty estimation and attenuation techniques in PMSM drives—A survey," *IEEE Trans. Ind. Electron.*, vol. 64, no. 4, pp. 3273–3285, Apr. 2017.
[18] Z. Wang and Z. Wu, "Nonlinear attitude control scheme with disturbance observer for flexible spacecrafts," *Nonlinear Dyn.*, vol. 81, nos. 1–2, pp. 257–264, Jul. 2015.
[19] Z. Wang, Z. Wu, and Y. Du, "Adaptive sliding mode backstepping control for entry reusable launch vehicles based on nonlinear disturbance observer," *Proc. Inst. Mech. Eng., G, J. Aerosp. Eng.*, vol. 230, no. 1, pp. 19–29, Jan. 2016.
[20] Z. Pu, R. Yuan, J. Yi, and X. Tan, "A class of adaptive extended state observers for nonlinear disturbed systems," *IEEE Trans. Ind. Electron.*, vol. 62, no. 9, pp. 5858–5869, Sep. 2015.
[21] H. Wang, Y. Huang, and C. Xu, "ADRC methodology for a quadrotor UAV transporting hanged payload," in *Proc. IEEE Int. Conf. Inf. Automat. (ICIA)*, Aug. 2016, pp. 1641–1646.
[22] Y. Xia, F. Pu, S. Li, and Y. Gao, "Lateral path tracking control of autonomous land vehicle based on ADRC and differential flatness," *IEEE Trans. Ind. Electron.*, vol. 63, no. 5, pp. 3091–3099, May 2016.
[23] K. K. Busawon and P. Kabore, "Disturbance attenuation using proportional integral observers," *Int. J. Control*, vol. 74, no. 6, pp. 618–627, Apr. 2001.
[24] Z. Gao, T. Breikin, and H. Wang, "Discrete-time proportional and integral observer and observer-based controller for systems with both unknown input and output disturbances," *Optim. Control Appl. Methods*, vol. 29, no. 3, pp. 171–189, May 2008.
[25] T. Madani and A. Benallegue, "Sliding mode observer and backstepping control for a quadrotor unmanned aerial vehicles," in *Proc. Amer. Control Conf.*, vol. 13, Jul. 2007, pp. 2462–2467.
[26] A. Benallegue, A. Mokhtari, and L. Fridman, "High-order sliding-mode observer for a quadrotor UAV," *Int. J. Robust Nonlinear Control*, vol. 18, nos. 4–5, pp. 427–440, 2008.
[27] D. Ginoya, P. D. Shendge, and S. B. Phadke, "Sliding mode control for mismatched uncertain systems using an extended disturbance observer," *IEEE Trans. Ind. Electron.*, vol. 61, no. 4, pp. 1983–1992, Apr. 2014.
[28] R. Yan and Z. Wu, "Attitude stabilization of flexible spacecrafts via extended disturbance observer based controller," *ACTA Astronautica*, vol. 133, pp. 73–80, Apr. 2017.
[29] C. Y. Chen, Y. D. Wang, and S. H. Li, "Generalized proportional integral observer-based composite control method for robotic thermal tactile sensor with disturbances," *Int. J. Adv. Robot. Syst.*, vol. 14, no. 3, pp. 1–10, Jun. 2017.
[30] A. A. Godbole, J. P. Kolhe, and S. E. Talole, "Performance analysis of generalized extended state observer in tackling sinusoidal disturbances," *IEEE Trans. Control Syst. Technol.*, vol. 21, no. 6, pp. 2212–2223, Nov. 2013.
[31] Y. J. Zhang, J. Zhang, L. Wang, and J. B. Su, "Composite disturbance rejection control based on generalized extended state observer," *ISA Trans.*, vol. 63, pp. 377–386, Jul. 2016.
[32] J. Han, "From PID to active disturbance rejection control," *IEEE Trans. Ind. Electron.*, vol. 56, no. 3, pp. 900–906, Mar. 2009.
[33] W. Wang and Z. Gao, "A comparison study of advanced state observer design techniques," in *Proc. Amer. Control Conf.*, vol. 6, Jun. 2003, pp. 4754–4759.
[34] A. Chovancová, T. Fico, P. Hubinský, and F. Duchoň, "Comparison of various quaternion-based control methods applied to quadrotor with disturbance observer and position estimator," *Robot. Auton. Syst.*, vol. 79, pp. 87–98, May 2016.
[35] S. Bouabdallah and R. Siegwart, "Full control of a quadrotor," in *Proc. IEEE/RSJ Int. Conf. Intell. Robots Syst.*, vol. 9, Oct./Nov. 2007, pp. 153–158.
[36] S. L. Waslander and C. Wang, "Wind disturbance estimation and rejection for quadrotor position control," in *Proc. AIAA Infotech@Aerospace Conf. AIAA Unmanned, Unlimited Conf.*, 2009, pp. 1–14.
[37] Y.-M. Chen, Y.-L. He, and M.-F. Zhou, "Decentralized PID neural network control for a quadrotor helicopter subjected to wind disturbance," *J. Central South Univ.*, vol. 22, no. 1, pp. 168–179, Jan. 2015.
[38] S. Li and M. Zhong, "High-precision disturbance compensation for a three-axis gyro-stabilized camera mount," *IEEE/ASME Trans. Mechatronics*, vol. 20, no. 6, pp. 3135–3147, Dec. 2015.
[39] J. Tatsumi and Z. Gao, "On the enhanced ADRC design with a low observer bandwidth," in *Proc. 32nd Chin. Control Conf. (CCC)*, Jul. 2013, pp. 297–302.
[40] Q. Quan and X. Dai. *Flight Performance Evaluation of UAVs*. Accessed: Mar. 20, 2018. [Online]. Available: http://flyeval.com/
[41] C. Wang, B. Song, P. Huang, and C. Tang, "Trajectory tracking control for quadrotor robot subject to payload variation and wind gust disturbance," *J. Intell. Robot. Syst.*, vol. 83, no. 2, pp. 315–333, Aug. 2016.
[42] L. Meier, P. Tanskanen, L. Heng, G. H. Lee, F. Fraundorfer, and M. Pollefeys, "PIXHAWK: A micro aerial vehicle design for autonomous flight using onboard computer vision," *Auton. Robots*, vol. 33, nos. 1–2, pp. 21–39, Aug. 2012.
[43] L. Meier, P. Tanskanen, F. Fraundorfer, and M. Pollefeys, "The PIXHAWK open-source computer vision framework for MAVs," in *Proc. Int. Conf. Unmanned Aerial Vehicle Geomatics (UAV-G)*, vols. 1–38, pp. 13–18, 2011.

DI SHI received the B.E. degree in automatic control from Beihang University, Beijing, China, in 2011, where he is currently working toward the Ph.D. degree at the School of Instrumentation Science and Optoelectronics Engineering. His main research interest is flight control.

ZHONG WU received the B.E. degree in automatic control from the North University of China, Taiyuan, China, in 1992, the M.E. degree in industrial automation from Tianjin University, Tianjin, China, in 1995, and the Ph.D. degree in control theory and control engineering from the Beijing Institute of Control Engineering, Beijing, China, in 1998.

He is currently a Professor with the School of Instrumentation Science and Optoelectronics Engineering, Beihang University, Beijing. His research interests include drive and control of servo systems and guidance and control of spacecrafts.

WUSHENG CHOU was born in Xinjiang, China, in 1969. He received the B.S. and M.S. degrees in electrical engineering and the Ph.D. degree in mechanical engineering from Tianjin University, Tianjin, China, in 1990, 1995, and 1998, respectively.

He is currently a Professor with the School of Mechanical Engineering and Automation, Beihang University, Beijing, China. His main research interests include industrial automation, embedded control, and mechatronics.